

# Changes in optical properties of tissue during acute wound healing in an animal model

## Elisabeth S. Papazoglou

Drexel University  
School of Biomedical Engineering  
Philadelphia, Pennsylvania

## Michael S. Weingarten

Drexel University College of Medicine  
Department of Surgery  
Philadelphia, Pennsylvania

## Leonid Zubkov

## Michael Neidrauer

## Linda Zhu

Drexel University  
School of Biomedical Engineering  
Philadelphia, Pennsylvania

## Som Tyagi

Drexel University  
Department of Physics  
Philadelphia, Pennsylvania

## Kambiz Pourrezaei

Drexel University  
School of Biomedical Engineering  
Philadelphia, Pennsylvania

## 1 Introduction

It is established that wounds, burns, and lesions need oxygen to heal and that ischemic conditions represent impaired healing environments.<sup>1-6</sup> Therefore, we hypothesize that by measuring oxygenated hemoglobin, deoxygenated hemoglobin, and oxygen saturation it would be possible to predict wound healing. Current methods in clinical wound care practice rely on estimates of the surface area by measuring length and width of the lesion.<sup>7</sup> These methods are highly subjective and more importantly cannot assess the probability of wound healing in impaired environments, such as in chronic wounds due to diabetes, venous ulcers, and others.<sup>8</sup> Invasive monitoring based on biopsies could provide information about the physiology and biochemistry of healing but is invasive and impractical; monitoring based on wound fluid is controversial due to debates over appropriate correlation of wound fluid composition to wound tissue.<sup>9-11</sup>

At present, various optical methods have been proposed and can be used for determining parameters representing skin injury or for monitoring the healing processes. Most optical methods are noninvasive and relatively inexpensive and as

**Abstract.** Changes of optical properties of wound tissue in hairless rats were quantified by diffuse photon density wave methodology at near-infrared frequencies. The diffusion equation for semi-infinite media was used to calculate the absorption and scattering coefficients based on measurements of phase and amplitude with a frequency domain device. There was an increase in the absorption and scattering coefficients and a decrease in blood saturation of the wounds compared with the nonwounded sites. The changes correlated with the healing stage of the wound. The data obtained were supported by immunohistochemical analysis of wound tissue. These results verified now by two independent animal studies could suggest a noninvasive method to detect the progress of wound healing. © 2008 Society of Photo-Optical Instrumentation Engineers. [DOI: 10.1117/1.2960952]

**Keywords:** near infrared spectroscopy (NIRS); diffuse photon density wave; wounds; oxygenated hemoglobin; deoxygenated hemoglobin; blood saturation.

Paper 07271RR received Jul. 20, 2007; revised manuscript received Jan. 27, 2008; accepted for publication Feb. 14, 2008; published online Aug. 26, 2008.

such offer major advantages compared with invasive methods.<sup>12-15</sup>

Different modifications of diffuse reflectance spectroscopy (DRS)<sup>13,14,16,17</sup> have become the most common methodology in diagnostic application for wounds, burns, and lesions. Diffuse reflectance spectroscopy has been used extensively for evaluating skin changes at superficial depths up to 1 mm, because with a typical broad range wavelengths source of incident light (400 to 1500 nm) the strong absorption exhibited by the tissue inhibits optical probing of deeper layers. Using specialized algorithms to fit DRS re-emission spectra to phantoms and model systems, many investigators obtained important information about the depth of burn injuries,<sup>14-16</sup> sun damage,<sup>18</sup> topical drug delivery,<sup>19</sup> and water content of the skin.<sup>20</sup>

In wound characterizations, the absence of significant depth penetration makes DRS data difficult to interpret. For example, DRS data from a significant number of wounds had to be collected to develop an empirical algorithm that could mimic a clinical wound assessment score that averages clinical observations.<sup>13</sup>

To probe deeper tissue depths with optical noninvasive methods, a different approach than DRS must be employed. The aim of diffuse photon density wave (DPDW)<sup>12,15</sup> meth-

Address all correspondence to Elisabeth S. Papazoglou, Drexel University School of Biomedical Engineering, 3141 Chestnut St., Philadelphia, Pennsylvania 19104. Tel: 215-895-4956; Fax: 215-895-4983; E-mail: elisabeth.s.papazoglou@drexel.edu.

odology of near infrared-spectroscopy (NIR) is to investigate tissue physiology from a few millimeters up to several centimeters below the skin or tissue surface. Specialized instruments must be built and operated at near-infrared wavelengths (650 to 850 nm) where the tissue appears as transparent as possible to that light; at these wavelengths, the absorption coefficient  $\mu_a$  of tissue is markedly lower than its value at visible wavelengths. The propagation of light in tissue is characterized by three phenomena: scattering, absorption, and reflection from various layers. The diffusion equation can describe light propagation in tissue if the characteristic distance between successive photon-scattering events (mean free path) is much less than  $1/\mu_a$  but larger than the wavelength of incident light. Then the dominant phenomenon of light propagation in tissue is multiple light scattering by cells, organelles, capillaries, and other interfaces and tissue structures. This is indeed the case at NIR wavelengths, where absorption of hemoglobin, water, and lipids is relatively very small (for hemoglobin less by a factor of 30 to 50 compared with absorption at 540 to 580 nm which is the range used in DRS methodologies for determining blood oxygenation). Furthermore, at a selected range of NIR wavelengths, the spectra of oxy- and deoxyhemoglobin are significantly different from each other and allow calculation of absolute concentrations of both types of hemoglobin and, consequently, oxygen saturation, if we know their extinction coefficients at the particular wavelengths. For special boundary conditions of the diffusion equation, simple closed form solutions can be obtained that allow calculation of absorption and scattering coefficients at specific NIR wavelengths from experimental data.

The DPDW method can yield quantitative information about blood oxygenation and blood volume, water, and lipid content, as well as qualitative information about changes of tissue structure. There are many biomedical applications where use of this noninvasive optical method could diagnose a wide range of medical pathologies. This includes cases where blood supply to the tissue changes significantly as a result of the disease, as in tumor angiogenesis.<sup>12,21–24</sup> In stroke, aneurysm, or brain damage and head injury, bleeding or ischemia can be determined by optical methods.<sup>25–28</sup> Additional applications lie in the areas of hemodynamics of human muscle, peripheral vascular diseases, control of photodynamic therapy, and monitoring of lesions.<sup>29–33</sup> The potential diagnostic value of using the DPDW methodology to characterize subcutaneous lesions and assess the necrotization depth of burns was discussed for the first time in a paper by Tromberg et al.<sup>31</sup> In a previous study,<sup>34</sup> we reported the use of DPDW methodology at NIR wavelengths to distinguish the optical properties of diabetic wounds from normal wounds in an animal model. In this study, we report the results of two new animal studies in which temporal changes in the optical properties of wound and nonwound tissue are monitored with DPDW methodology at NIR wavelengths throughout the course of wound healing. The absorption and scattering coefficients can be calculated, and blood oxygenation can be quantified by using the diffusion approximation with the semi-infinite boundary condition. Our approach has been to measure optical properties of the wound tissue *in vivo* and calculate tissue oxygenation using the optical absorption coefficient. Because depth penetration is accomplished at relevant physiological depths, there is no need for empirical fit-

ting of spectroscopic data. Our data obtained from *in vivo* measurements strengthen and support the conclusions of Tromberg et al.<sup>31</sup> on the advantages of using DPDW to study necrotic burn tissue or skin lesions. Differences in tissue optical properties between the wound and nonwounded site during the course of healing can reveal information about physiological changes of the tissue, such as its inflammatory state and its rate of healing. The results presented here indicate that this NIR method would be highly useful in monitoring and quantifying the wound healing process.

## 2 Materials and Methods

### 2.1 Optical Methods

The frequency domain DPDW instrument illuminated the animal tissue with four diode lasers in the NIR window at wavelengths of 685, 780, 830, and 950 nm, with its intensity modulated by a radio frequency  $\omega=70$  MHz.<sup>34</sup> A schematic of the device and a detailed description can be found elsewhere.<sup>34</sup> Backscattered light was delivered to four detector blocks based on avalanche photodiodes (APD) and quadrature ( $I/Q$ ) demodulators. The  $I$  and  $Q$  signals in each detector were measured; these were determined by the attenuated amplitude  $A_{att}$  and phase shift  $\Theta_{log}$  of the registered scattered light. The output power at the end of the source fiber ranges from 5 to 7 mW, for all four wavelengths.

The diffusion approximation can be used to calculate absorption  $\mu_a$  and reduced scattering  $\mu'_s$  coefficients of tissue based on the solution of the time-dependent diffusion equation assuming a semi-infinite tissue geometry.<sup>35,36</sup> We used the closed form analytical solutions to the diffusion equation for calculating the optical properties of animal tissue.<sup>36</sup> The so-called extrapolated condition for semi-infinite media is a good approximation in noninvasive clinical applications where the fluence rate is nonzero at the boundary.

During this diffusion and “snake-like” propagation of light in the tissue, light is attenuated in intensity and also subjected to a phase shift that reflects the mean flight time of photons through the strongly scattering medium (tissue). The reduced scattering coefficient is defined as a function of the scattering coefficient  $\mu_s$ ,  $\mu'_s = \mu_s(1-g)$ , where the average cosine angle of scattering  $g \sim 0.9$  for biological tissue and its inverse is defined as the mean transport length  $l^*$ . Usually after propagation of more than two or three  $l^*$ , photons have no memory of the incident direction of light; we can then assume that the radiance is quasi-isotropic.

For most biological tissues  $\mu'_s$  is between 5 and 15  $\text{cm}^{-1}$  and its value determines the design of the appropriate experimental probe. In our studies, we assumed that  $\mu'_s \sim 10 \text{ cm}^{-1}$  for animal tissue and designed an optimal probe. The scattering coefficient calculated from our studies was very close to the assumed value of 10  $\text{cm}^{-1}$ , corresponding to  $l^*$  around 1 mm. Because the smallest source-detector separation of our probe (4 mm) is larger than  $3 \cdot l^*$ , the diffusion approximation will be valid.

The optical fibers were inserted in a Teflon probe of length 25 mm and width 7 mm, with a separation between source and detector fibers of  $\rho=4, 8, 12,$  and 16 mm. It is possible to estimate the probable penetration depth of diffuse light  $D_v$  in the tissue as function of the source-detector separation  $\rho$  by

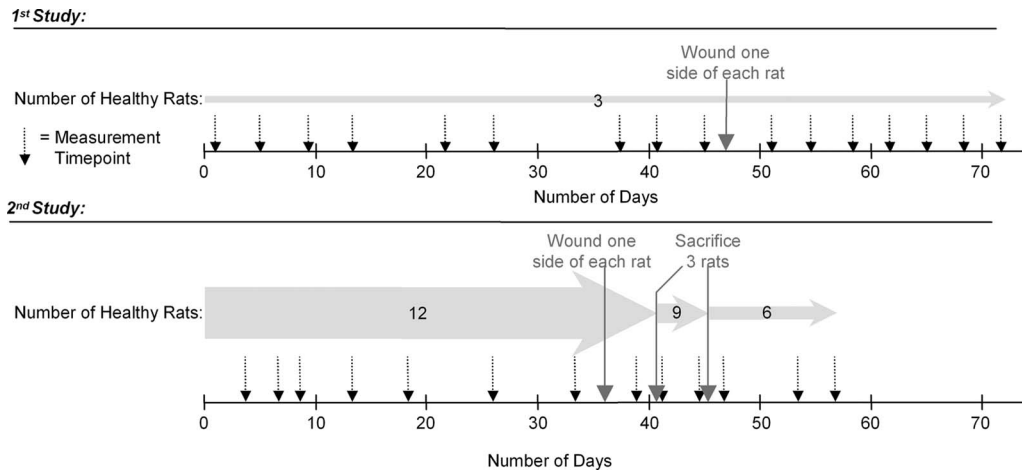


Fig. 1 Timeline of animal studies.

using diffusion theory. A detailed investigation of this problem can be found in Refs. 37 and 38, but a rule of thumb often applied is that  $D_v \sim (1/3 - 1/2) \rho$ .

## 2.2 Calibration Procedures

The measured intensity of scattered light  $A_{att}$  depends not only on the tissue properties, but also on the sensitivity of the APD, the coupling to the detectors fibers, the transmission of the optical fibers, and the gain of each detector block. The phase shift  $\Theta_{log}$  may be different in each channel because the optical and electrical signal delay depends on fiber length and coupling, the length of the RF coaxial cables, and any delays in the detector circuits. Instrument calibration is performed to allow us to separate variability due to the instrument hardware components from sample and measurement variability. An equidistant probe is constructed to conduct the first instrument calibration. The four detector fibers are inserted in a Teflon probe with the same source-detector separation of 12 mm. The probe is placed on the surface of a liquid optical phantom (Liposyn, Abbott Laboratories, Chicago, Illinois) that simulates tissue optical properties in a semi-infinite geometry. The set of calibration coefficients that equalizes the amplitude and phase of the second, third, and fourth detector relative to the first detector is determined. All subsequent experimental data are corrected using this set of calibration coefficients.<sup>34</sup>

It should be noted that the use of a Liposyn solution as an optical phantom for experiments that span several days is not the best approach, because the solution changes optical properties due to phase separation and degradation. An additional factor that contributes to operator variability when using Liposyn is the repeatability of placing the solid plastic probe exactly on the surface of the solution. Use of the semi-infinite approximation relies on perfect contact between the solid and liquid interface, without any air gap and also without immersing the probe in the liquid. Solid phantoms can overcome some of these challenges. Silicone optical phantoms were the method of choice for calibrating the NIR device because these models do not change optical properties during the time course of our experiments. Cylindrical phantoms made of silicone with dispersed particles of titanium dioxide to act as scatters and carbon black to act as an absorber were used.<sup>39</sup>

Cylinders with diameter of 90 mm and thickness of 45 mm were synthesized from silicone XP565 with activator (platinum catalyzed from Silicones Inc., High Point, North Carolina); TiO<sub>2</sub> particles with diameters between 0.9 and 1.6  $\mu\text{m}$  simulated tissue scattering, and carbon black acetylene, 50% compressed, 99.9+% (metals basis) (diameter=0.042  $\mu\text{m}$ ), simulated light absorption. Both TiO<sub>2</sub> and carbon black were obtained from Alfa Aesar (Ward Hill, Massachusetts).

We optimized the preparation of these models including intensity and time of mixing, the order of addition of the components, and the crosslinking reaction to ensure phantoms of desired composition with no air bubbles. We verified the absence of microbubbles by sectioning the phantoms in thin layers and observing their surfaces under an optical microscope.

Typical of any device that measures light intensity, our instrument has a limited range where the electrical output signal is proportional to the optical power of the input signal. A second calibration was conducted to define the region of saturation that occurs at an output signal of around 100 mV. The linearity range for the device used in this study was  $>50$  dB. Typical magnitudes of the  $I$  and  $Q$  demodulation signals were in the range of 2 to 70 mV. Offset for our instrument, defined as the signal measured without any light, was measured before every experiment on an animal and has not exceeded 500  $\mu\text{V}$  for any experiment, with an average value around 250  $\mu\text{V}$  throughout our studies. This calibration experiment allows us also to calculate the noise-equivalent power for our device, which was equal to 5 pW/Hz.

## 2.3 Animal Models

We have used hairless rats as the animal model for studying tissue optical properties during wound healing. This is a model that is widely used and accepted for studying skin and wound properties.<sup>40,41</sup> The absence of hair removes the complications of inflammation introduced by shaving the wound site and does not interfere with the optical measurements.

Animal procedures were conducted in accordance with the *Guide for the Humane Care and Use of Laboratory Animals*.<sup>42</sup> The experimental protocol was approved by Drexel University's Institutional Animal Care and Use Committee. During the

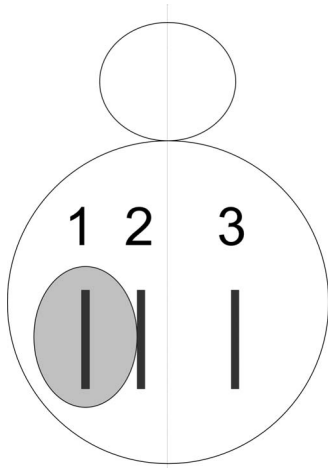


**Fig. 2** Probe placement locations (dark rectangles) in animal model. Each animal was wounded on the left dorsum, and measurements were performed on (1) the center of the wound, (2) the edge of the wound, and (3) healthy tissue on the right dorsum, symmetric to the wound location.

course of the study, all animals were supplied with food and water *ad libitum* and were housed in individual cages. We performed two independent studies as described below.

### 2.3.1 First study

Three female hairless Sprague Dawley rats, 5 to 6 weeks old and approximately 150 g each, were purchased from Charles River Laboratory (Wilmington, Massachusetts). A measurement protocol was developed over the course of 15 weeks, and when measurements began the rats weighed approximately 300 g each. The rats were monitored with NIR for 48 days (Fig. 1), with independent measurements taken usually every 3 to 4 days. On the 48th day, one quarter-sized (4.6 cm<sup>2</sup>) full thickness wound (Fig. 2) was inflicted on the left dorsal area of each animal to produce a wound animal model on all rats.

A full thickness wound is a superficial wound where the epidermis and dermis are removed to expose the underlying tissue. It is different from an incision wound, and it heals by contraction. Sixteen series of optical measurements were performed on the wound and on skin bordering the edge of the wound. Symmetrical measurements were performed on the right dorsal side of all animals (Fig. 2).

### 2.3.2 Second study

Twelve healthy rats identical to the ones in the first study were purchased and allowed to acclimate to their surroundings for four weeks until they weighed approximately 200 g each. Baseline NIR data were collected on all rats for 33 days (Fig. 1), with independent measurements taken every 3 to 4 days. On day 36, a full thickness wound 4.6 cm<sup>2</sup> was made using a sterile technique in an animal surgical suite. One wound was inflicted on the left side of the dorsal area of each animal. The right side of each animal was left unwounded to provide a control site. The NIR measurements were performed on the wounds and control sites until day 57 (Fig. 2), when the wounds were completely re-epithelialized. The wound surgery

and all optical measurements were performed using isoflurane and oxygen anesthesia administered via face mask to prevent the animals from moving. It was necessary to anesthetize the animals to eliminate motion artifacts before performing NIR measurements. Animals were measured as soon as they stopped moving and NIR measurements lasted 5 min at most. All wounds were covered with a Tegaderm (3M, Minneapolis, Minnesota) sterile transparent dressing after wound surgery and between optical measurements. After surgery all rats were fitted with “Elizabethan” type collars to prevent them from scratching their wounds.

## 2.4 Immunohistochemistry

### 2.4.1 Tissue excision

During the second study, three rats were sacrificed by CO<sub>2</sub> suffocation on days 5 and 10 after wound surgery, respectively. The wound and surrounding skin were completely excised, as was the area of the dorsum contralateral to the wound. This procedure was repeated for the remaining six rats on day 21 after wound surgery. All excised tissue was immediately frozen at -80 °C until needed.

### 2.4.2 Blood vessel staining

Lectin staining (a sugar binding protein of nonimmune origin that agglutinates cells or precipitates glycoconjugates) was used to stain vessels in the tissue and visualize vascularization. Lectin can be used as a marker of angiogenesis because it binds to endothelial cells and reveals the overall vascular architecture.<sup>43,44</sup> Briefly, sections were washed in 1× phosphate buffered solution (PBS), Carlsbad, California for 10 min after rehydration. Sections were stained with Alexa Fluor 488 conjugated lectin (L2-1415 Invitrogen) for 30 min in the dark with a concentration at 1:250 and washed with 1 × PBS three times for 5 min each.

## 3 Results

### 3.1 Baseline

The stability and accuracy of the frequency domain NIR instrument used in the study is demonstrated in Fig. 3, which tracks the absorption and reduced scattering coefficients over the course of 50 days measured in silicone phantoms. Standard error remained at less than 4% throughout the period of the study.

To be able to detect the small changes in optical properties occurring during wound healing, the NIR device used must exhibit very good stability. Otherwise it would be impossible to discern systematic device drift from actual physiological changes. The 48-day and 36-day periods of *in vivo* measurements prior to wound surgery in the first and second studies, respectively, allowed us to determine with high consistency the local values of  $\mu_a$  and  $\mu'_s$  for the animals.

These form the baseline measurements for assessing changes in optical properties during our wound healing studies. Combined results of baseline measurements for  $\mu_a$  and  $\mu'_s$  from both animal studies are shown in Fig. 4 for 685 nm. The error bars in Fig. 4 indicate the between-animal variation, which was less than 15% percent of the average values of  $\mu_a$  and  $\mu'_s$  for each time point in study 2. Similar results were obtained for 785- and 830-nm measurements. Baseline mea-

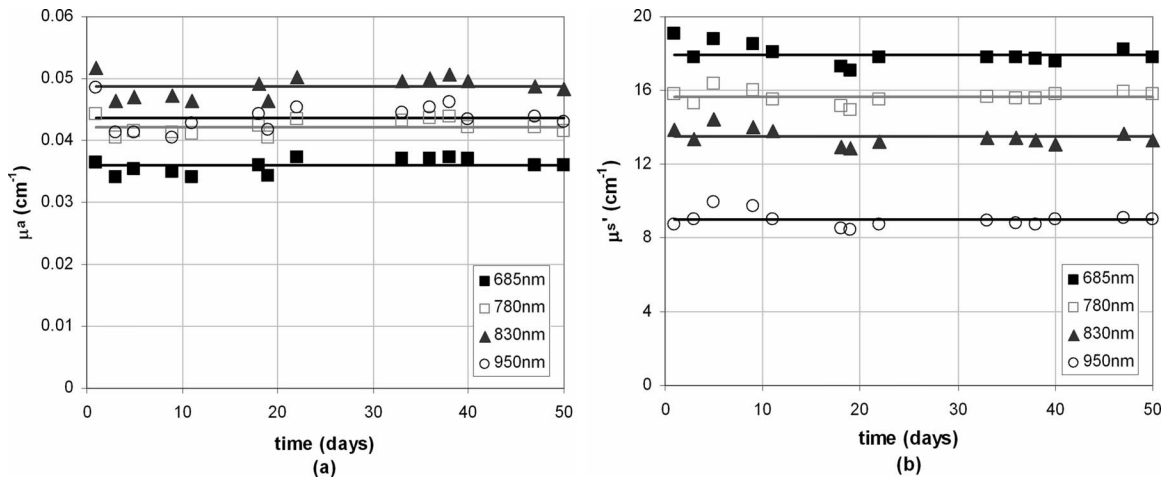


**Fig. 3** Daily average values of (a)  $\mu_a$  and (b)  $\mu_s'$  in a silicone optical phantom over a 50-day period. Each point represents the average of measurements taken on the same day. Solid lines represent average values for the entire measurement period.

measurements for three representative rats are presented in Fig. 5. Within-animal variation was less than 15% of the average values of  $\mu_a$  and  $\mu_s'$  for each animal in the second study.

If we compare these *in vivo* data with those obtained from phantoms it is clear that in addition to the noise from the laser

diodes, electronics, and fibers, being common to both *in vitro* and *in vivo* measurements, additional noise emanates from physiological changes in the animal tissue during our experiments. Several reasons may be responsible for such changes. The size of the rat is small, even compared with a 2-cm

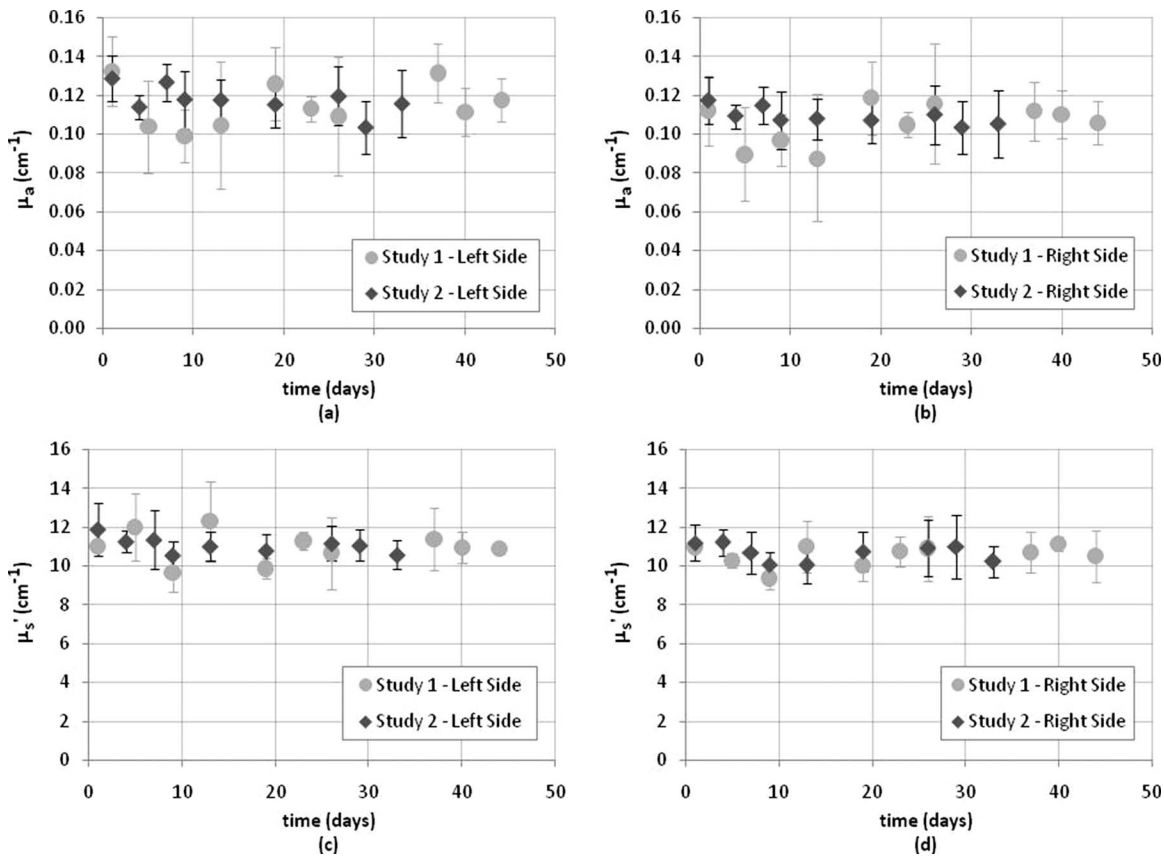


**Fig. 4** Average absorption and scattering coefficients for all animals measured as a function of time. Baseline values of (a) left dorsal  $\mu_a$ , (b) right dorsal  $\mu_a$ , (c) left dorsal  $\mu_s'$ , and (d) right dorsal  $\mu_s'$  at 685 nm from study 1 and study 2. Each point represents the average of measurements taken on that day; error bars represent the standard deviation. In both studies, baseline optical measurements were taken at symmetric locations on the left and right dorsa of each animal. The average data of baseline stability obtained during the second study (black points) is a better indicator of device stability because of the higher number of animals ( $n=12$ ) compared to  $n=3$  in the first study (gray points).

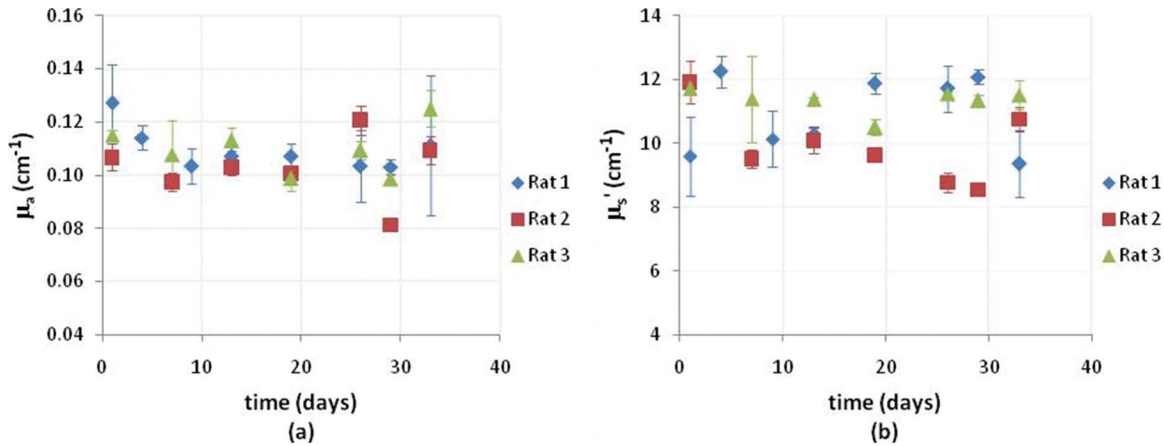


**Fig. 5** Left dorsal baseline values of (a)  $\mu_a$  and (b)  $\mu_s'$  from three representative rats. Each point represents the average of three measurements and error bars represent the standard deviation.

probe. The rats were anesthetized during measurements and unable to move; however, breathing may have contributed to unintended change in probe positioning. The food supply was provided *ad libitum*, and this may have affected the amount of blood at the measurement sites at various times. Rats have been growing during the period of baseline measurements, and therefore, a slightly different tissue volume was examined as time went on.

Attention is drawn to the fact that the absorption coefficient is systematically higher for the left dorsal side as compared with the right one, for all animals at all time points (Fig. 4). During the second study, the differences in  $\mu_a$  between the two sides range from 0.01 to 0.015 cm<sup>-1</sup> and this may be due to asymmetry in the animal physiology. We only report this observation for the second study because in this case we have more representative statistics.

### 3.2 Optical Properties during Wound Healing

In our experiments, wound size was determined by calculating wound surface area from cross-polarized digital images, which were taken at the same time the NIR data was collected. The image analysis tool IMAGE PRO (Media Cybernetics, Silver Spring, Maryland) was used to calculate the area of each wound. Although the original size of each wound was large relative to the size of the rat, the wound healing rate was very fast for this model (as with all healthy animals) and is evidence of the intense physiological changes in the animal during healing. A normalized wound area was obtained by calculating the ratio of wound area each day to the initial wound area on the day of surgery (day 0). Average normalized wound areas are presented in Fig. 6 (study 2). Wound healing rate in this animal model exhibits a nonlinear behavior as reported by Chen et al.<sup>2</sup> From our data, we can observe the healing rate is fast between days 3 and 10 and then decelerates at time points 15 to 24 to achieve full wound closure.

We monitored the change of optical properties during wound healing for all animals. Changes of optical properties at 685 nm as a result of our experiments are shown in Fig. 7. The absorption coefficient of the wound is increasing during wound healing and asymptotically approaches a value that is higher by 0.035 to 0.040 cm<sup>-1</sup>, or 35% to 40% (Fig. 7, open

squares and triangles) compared with the nonwounded site (Fig. 7, filled diamonds) throughout the experiment. The difference in  $\mu_a$  between wound and nonwound tissue is statistically significant ( $p < 0.01$ ) after day 5. The difference in  $\mu_s'$  between wound and nonwound tissue is statistically significant ( $p < 0.05$ ) after day 3. Similarly shaped healing curves were observed at other wavelengths, with  $\mu_a$  at 780 nm increasing by 0.030 to 0.035 cm<sup>-1</sup> (approximately 35%) and  $\mu_a$  at 830 nm increasing by 0.040 to 0.045 cm<sup>-1</sup> (approximately 40%) when compared with the nonwounded site.

Increasing values of  $\mu_a$  as the wound is healing could be due to angiogenesis and neovascularization, and this was supported by immunohistochemical analysis where vessel ingrowth increased with time in lectin-stained images of blood vessels (Fig. 8—endothelial cells are stained with green color).

As may be seen from Fig. 7, the values of  $\mu_a$  obtained from measurements on the center of the wounds are identical (within experimental error) to the absorption coefficients ob-

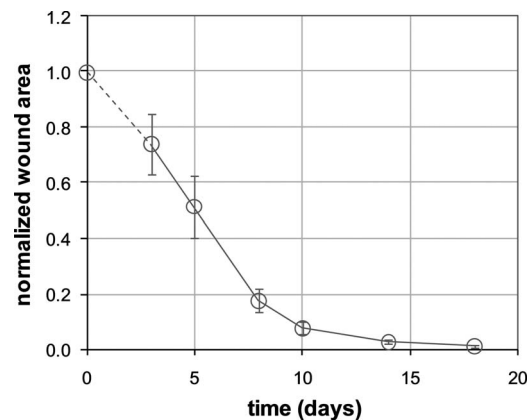


**Fig. 6** Normalized wound area as a function of healing time for rats in study 2. Each point represents the average of all rats ( $n=12$ ) and error bars represent the standard deviation. Wound surgery was performed on day 0. The data points on days 0 and 3 are connected by a dashed line because from Chen et al. (Ref. 2) it is known that the rate exhibits highly nonlinear behavior prior to day 3.

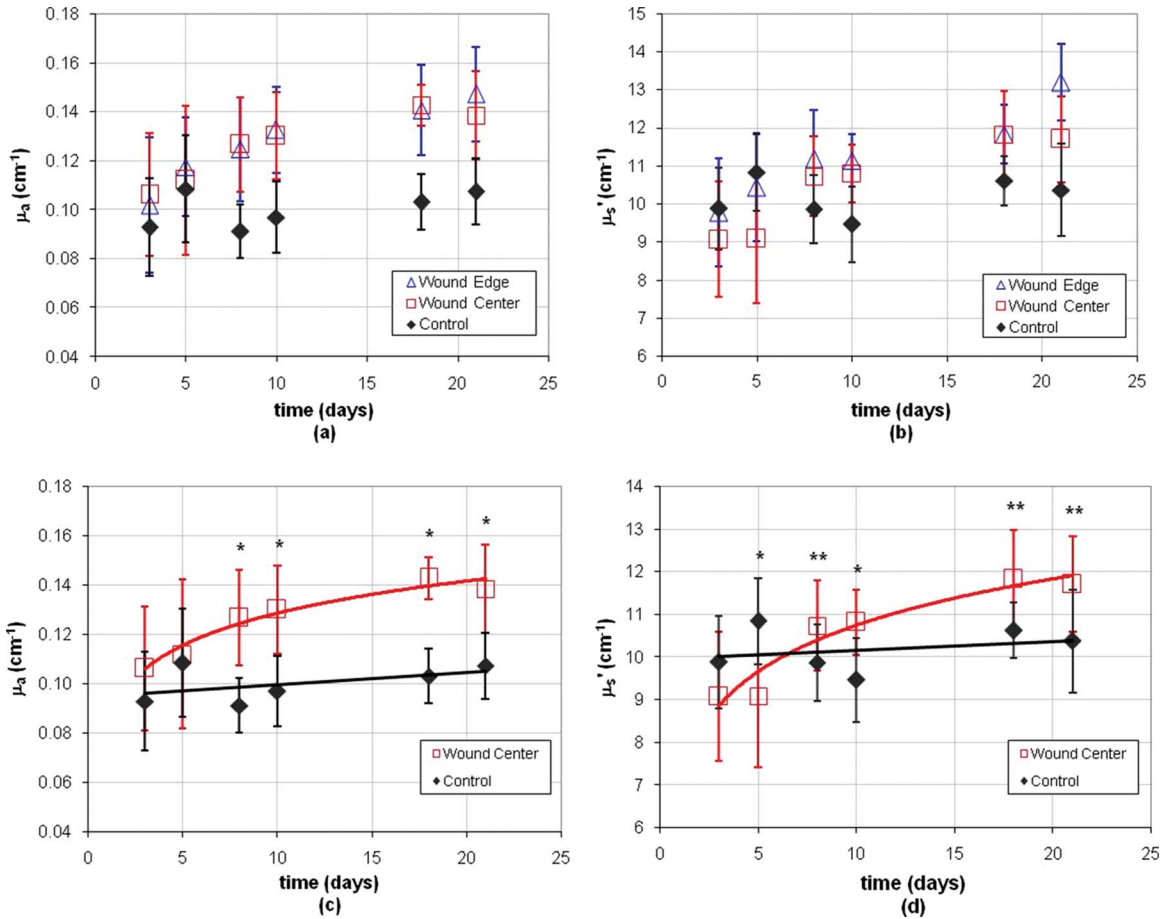


**Fig. 7** (a)  $\mu_a$  and (b)  $\mu'_s$  at 685 nm during wound healing (average  $\pm$  standard deviation) for animals in study 2. Wound surgery was performed on day 0. Open triangles represent measurements taken on the edges of the wounds; open squares represent measurements taken at the center of the wounds; and closed 20 diamonds represent control measurements on the nonwounded site. (c)  $\mu_a$  and (d)  $\mu'_s$  at 685 nm during wound healing (average  $\pm$  standard deviation) for animals in study 2. Wound surgery was performed on day 0. Open squares represent measurements taken at the center of the wounds, and closed diamonds represent control measurements on the nonwounded site. Two-tailed paired  $t$ -tests were performed to compare wound center and control data at each time point (\* $p < 0.01$ , \*\* $p < 0.05$ ).

tained from measurements of the periwound area particularly for the first several measurements when the wounds are large in size compared with the probe size.

This remained consistent in both animal studies and can be explained by the geometry of our experiments. Studies of photon penetration depth at these wavelengths with geometry similar to the one we have used have shown that a probe having a source-detector separation of 16 mm registers scattered light from a tissue volume up to 5 mm beneath its surface.<sup>38</sup> The similarity between optical properties measured

at the wound center and wound periphery provides evidence that the measured tissue is located beneath the skin's surface, and therefore overlapping tissue volumes are interrogated as the probe is positioned on the center or the periphery of the wound. This observation may have clinical utility because it indicates that a wound could be monitored without the fiber optic probe touching directly the surface of an open wound.

The data on Fig. 7 suggest that during normal wound healing, the optical properties of tissue at NIR wavelengths change measurably, and therefore, healing may be followed by measuring changes of the absorption coefficient of the wound. Oxyhemoglobin concentration ( $[HbO_2]$ ) and deoxyhemoglobin concentration ( $[Hb]$ ) were calculated from the values of  $\mu_a$  and  $\mu'_s$  using a modified form of the Beer-Lambert equation:

$$\epsilon_{Hb}^\lambda [Hb] + \epsilon_{HbO_2}^\lambda [HbO_2] + \mu_{a,H_2O}^\lambda [\% H_2O] = \mu_{a,measured}^\lambda \quad (1)$$

where  $\epsilon_{Hb}^\lambda$  and  $\epsilon_{HbO_2}^\lambda$  are the molar extinction coefficients of deoxy- and oxyhemoglobin,<sup>45</sup>  $\mu_{a,H_2O}^\lambda$  is the absorption coefficient of pure water,<sup>46</sup> and  $[\% H_2O]$  is the percentage of water

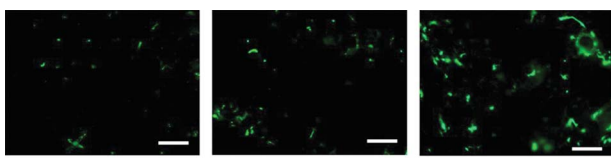


**Fig. 8** Lectin-stained images of wound tissue on (a) day 5, (b) day 10, and (c) day 21 after wound surgery. Vascular structures appear bright against a black ground. The number and size of vascular structures increases as the wound heals. Scale bars represent 25  $\mu\text{m}$ .

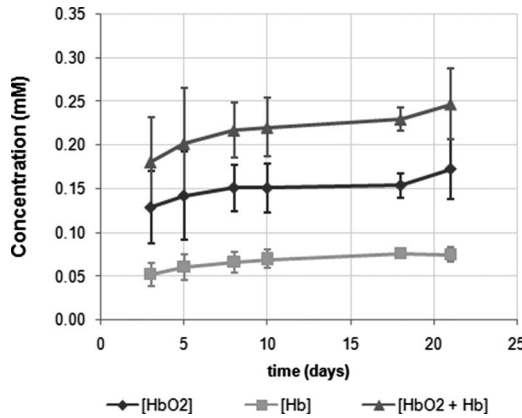


**Fig. 9** Mean  $\pm$  standard deviation of oxyhemoglobin [ $HbO_2$ ], deoxyhemoglobin [ $Hb$ ], and total hemoglobin [ $HbO_2 + Hb$ ] during wound healing for animals in study 2. Wounds were inflicted on day 0.

in the measured tissue, which we assumed to be 70%. Mean hemoglobin values increased during wound healing, as shown in Fig. 9. Within the accuracy limits of our experiment, we did not obtain any significant change in oxygen saturation during the course of wound healing, as shown in Fig. 10. Oxygen saturation is defined as  $SO_2 = [HbO_2] / [HbO_2 + Hb]$ , where  $HbO_2$  and  $Hb$  are the concentrations of oxygenated and deoxygenated hemoglobin.

This small change supports the findings by Hunt et al.,<sup>47</sup> who suggested that oxygen saturation is not a sensitive measure of wound healing because hemoglobin delivery to the wound environment is disrupted by microvasculature damage, vasoconstriction, and clotting in the area surrounding a wound.<sup>48</sup> However, the optical properties of tissue change measurably in this animal model during wound healing in contrast to the insignificant change of oxygen saturation. Therefore, tissue absorption coefficients may have adequate sensitivity to be good global indicators of changes during wound healing.

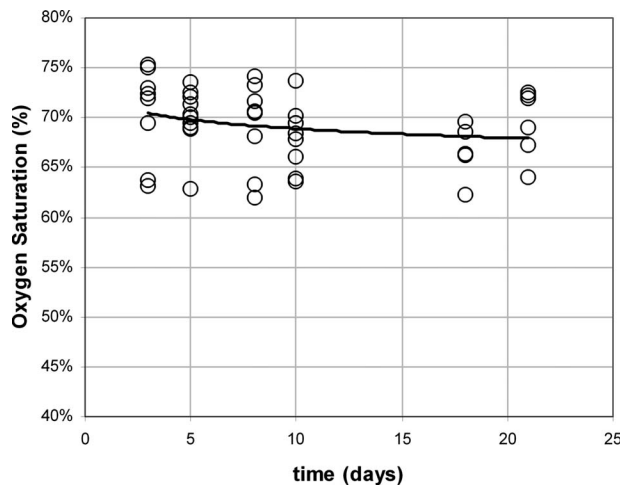


**Fig. 10** Oxygen saturation during wound healing for animals in study 2. Wounds were inflicted on day 0.

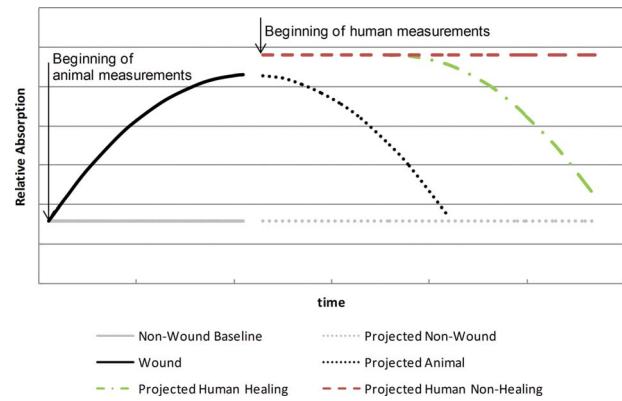


**Fig. 11** Hypothesized clinical wound healing curve. Black lines represent the result of the animal study shown in Fig. 7. Dashed and dash-dotted lines are hypothesized curves for healing and nonhealing wounds. The amount of time required for the healing curve to converge to the baseline is not known at this point.

#### 4 Discussion and Conclusion

In the NIR region, the change of the absorption coefficient  $\mu_a$  reflects the variation in oxygenated and deoxygenated hemoglobin concentration because hemoglobin is the main absorption chromophore at the wavelength range 680 to 850 nm along with water and lipids.

The NIR absorption coefficient during wound healing (Fig. 7) increases on the wound side by 0.020 to 0.035  $cm^{-1}$ , and total hemoglobin concentration increases by 0.06 to 0.07 mM (Fig. 9). This means that during normal healing, the optical properties of tissue change measurably in this animal model as a result of a 30% to 35% difference in blood volume between the wound side and the control side. It would be important to monitor how the absorption coefficient returns to normal levels (prewound) after the tissue has remodeled fully and the system has recovered from the wound perturbation.

Our results demonstrating baseline differences  $\mu_a$  between the left and right dorsal side highlight the importance of selecting a control site with well-understood optical properties relative to the wound site, and that a contralateral position may not be the optimal control site. In a clinical application, optical measurements occur on patients with already existing wounds. Therefore, we would be looking at trends of absorption and scattering coefficients of the wound sites over time. Because we will be not be able to compare the optical properties of patient wounds to any prewound baseline, in the clinic we will be selecting a control site with stable optical properties. The optical properties of this control site will be used to establish the baseline stability of a human study. In the framework of our model, the absorption coefficient should decrease if proper healing is occurring, as is demonstrated in Fig. 11.

To further analyze our results, we performed two-tailed  $t$ -tests to understand how our optical data reflect the process of wound healing in this animal model. The  $t$ -test allows us to differentiate values of absorption and scattering over time with statistical significance and finer detail compared with a simple comparison of average values and their standard deviations.

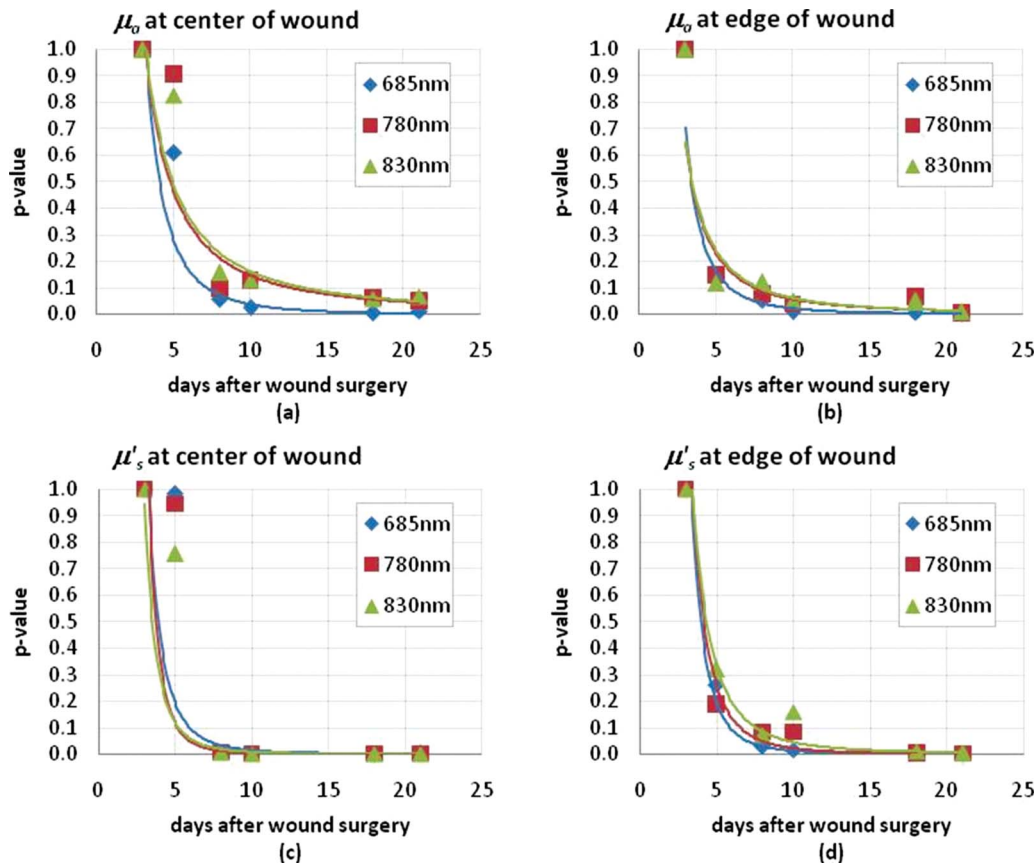


**Fig. 12** Two-tailed, unpaired *t*-tests were used to compare the average optical coefficients at each time point to the average optical coefficients on day 3. The resulting *p* values are shown as a function of time. (a)  $\mu_a$  at center of wound, (b)  $\mu_a$  at edge of wound, (c)  $\mu'_s$  at center of wound, and (d)  $\mu'_s$  at edge of wound.

Absorption and scattering coefficients from day 3 of wound healing were compared with data from each subsequent time point using *t*-tests. The results, presented in Fig. 12, show that the *p* value obtained for the 685-nm absorption coefficient becomes very small (at the level of 0.01) at day 18 for the wound center and at day 8 for the wound edge. The absorption at 685 nm is due mostly to deoxygenated hemoglobin corresponding to the tissue metabolic activity. Therefore, at the wound center, there may be a time lag for significant metabolic activity. At the other two wavelengths—785 and 830 nm—the *p* values are systematically higher, demonstrating that 685-nm absorption may be a more sensitive indicator of metabolic changes that occur during wound healing than absorption at other wavelengths and oxygen saturation. Another very important conclusion from these data is that the *p* value decreases earlier for the wound edge than it does for the wound center. These results are in agreement with a healing wound model where healing starts from the edges and the wound heals by contraction. This is the wound healing mode followed by this animal model where healing starts from “around” the wound, with increased metabolic activity, and the wound center is the last location where epithelialization (new skin) is formed.

We would like to extend these animal *in vivo* studies to measurements of wounds in patients. The demonstrated baseline stability of the device makes it possible to use this

method in a clinical setting where measurements are performed on chronic wounds spanning periods of 6 to 12 months. Our results suggest that the NIR methodology and instrument we developed is stable and capable of detecting changes to optical properties connected to wound healing. This quantitative noninvasive method could complement the current practice of monitoring wound healing based on visual observation and measurement of wound size to improve the quality of wound care.

In summary, our *in vivo* studies using the hairless rat animal model have demonstrated that the absorption coefficient of tissue at all NIR wavelengths probed (680, 785, 830) is higher in the wound compared with the unwounded side of animals, which corresponds to increased vascularization. The observed differences in  $\mu_a$  between the wounded and unwounded side of animals can be attributed to the traditional chromophores of oxygenated and deoxygenated hemoglobin, because we did not find any evidence of a different type of tissue chromophore in these wavelengths. Our results also demonstrated that the right and left side of these animals are slightly asymmetric in their optical properties and this must be further explored for long-term wound healing studies.

#### Acknowledgments

The authors would like to thank the Wallace H. Coulter Foundation and the U.S. Army Medical Research Acquisition Ac-

tivity for their generous support of this project. This research was funded by The U.S. Army Medical Research Acquisition Activity, and the office at 820 Chandler Street, Fort Detrick, Maryland 21702-5014 is the awarding and administering acquisition office. This investigation was funded under a U.S. Army Medical Research Acquisition Activity; Cooperative Agreement W81XWH 04-1-0419. The content of the information herein does not necessarily reflect the position or the policy of the U.S. government or the U.S. Army and no official endorsement should be inferred.

## References

- H. Brem and M. Tomic-Canic, "Cellular and molecular basis of wound healing in diabetes," *J. Clin. Invest.* **117**(5), 1219–1222 (2007).
- C. Chen, G. S. Schultz, M. Bloch, P. D. Edwards, S. Tebes, and B. A. Mast, "Molecular and mechanistic validation of delayed healing rat wounds as a model for human chronic wounds," *Wound Repair Regen* **7**(6), 486–494 (1999).
- R. J. Ehrlichman, B. R. Seckel, D. J. Bryan, and C. J. Moschella, "Common complications of wound healing. Prevention and management," *Surg. Clin. North Am.* **71**(6), 1323–1351 (1991).
- D. K. Harrison, "Optical measurements of tissue oxygen saturation in lower limb wound healing," *Adv. Exp. Med. Biol.* **540**, 265–269 (2003).
- P. Poredos, S. Rakovec, and B. Guzac-Salobir, "Determination of amputation level in ischaemic limbs using tcPO<sub>2</sub> measurement," *Vasc. Dis.* **34**(2), 108–112 (2005).
- H. K. Said, J. Hijjawi, N. Roy, J. Mogford, and T. Mustoe, "Transdermal sustained-delivery oxygen improves epithelial healing in a rabbit ear wound model," *Arch. Surg. (Chicago)* **140**(10), 998–1004 (2005).
- H. Charles, "Wound assessment: measuring the area of a leg ulcer," *Br. J. Nurs.* **7**, 765–772 (1998).
- R. Mani, "Science of measurements in wound healing," *Wound Repair Regen* **7**(5), 330–334 (1999).
- C. E. Davies, K. E. Hill, R. G. Newcombe, P. Stephens, M. J. Wilson, K. G. Harding, and D. W. Thomas, "A prospective study of the microbiology of chronic venous leg ulcers to reevaluate the clinical predictive value of tissue biopsies and swabs," *Wound Repair Regen* **15**(1), 17–22 (2007).
- S. L. Drinkwater, A. Smith, and K. G. Burnand, "What can wound fluids tell us about the venous ulcer microenvironment?" *Int. J. Lower Extrem. Wounds* **1**(3), 184–190 (2002).
- K. Lundqvist, H. Herwald, A. Sonesson, and A. Schmidtchen, "Heparin binding protein is increased in chronic leg ulcer fluid and released from granulocytes by secreted products of *Pseudomonas aeruginosa*," *Thromb. Haemostasis* **92**(2), 281–287 (2004).
- T. Durduran, R. Choe, J. P. Culver, L. Zubkov, M. J. Holboke, J. Giammarco, B. Chance, and A. G. Yodh, "Bulk optical properties of healthy female breast tissue," *Phys. Med. Biol.* **47**(16), 2847–2861 (2002).
- W. D. Schmidt, K. Liebold, D. Fassler, and U. Wollina, "Contact-free spectroscopy of leg ulcers: principle, technique, and calculation of spectroscopic wound scores," *J. Invest. Dermatol.* **116**(4), 531–535 (2001).
- M. G. Sowa, L. Leonardi, J. R. Payette, K. M. Cross, M. Gomez, and J. S. Fish, "Classification of burn injuries using near-infrared spectroscopy," *J. Biomed. Opt.* **11**, 054002 (2006).
- A. Yodh and B. Chance, "Spectroscopy and imaging with diffusing light," *Phys. Today* **48**(3), 34–40 (1995).
- K. M. Cross, L. Leonardi, J. R. Payette, M. Gomez, M. A. Levasseur, B. J. Schattka, M. G. Sowa, and J. S. Fish, "Clinical utilization of near-infrared spectroscopy devices for burn depth assessment," *Wound Repair Regen* **15**(3), 332–340 (2007).
- K. Liebold, D. Fassler, W. D. Schmidt, T. Kuhn, and U. Wollina, "In vivo spectroscopy in dermatology: methods and new fields of application," *J. Eur. Acad. Dermatol. Venereol* **14**(1), 1–4 (2000).
- R. Gillies, D. Moyal, S. Forestier, and N. Kollias, "Non-invasive in vivo determination of UVA efficacy of sunscreens using diffuse reflectance spectroscopy," *Photodermatol. Photoimmunol. Photomed.* **19**(4), 190–194 (2003).
- B. Sennhenn K. Giese, K. Plamann, N. Harendt, K. Kolmel "In vivo evaluation of the penetration of topically applied drugs into human skin by spectroscopic methods," *Skin Pharmacol.* **6**(2), 152–160 (1993).
- H. Arimoto, M. Egawa, and Y. Yamada, "Depth profile of diffuse reflectance near-infrared spectroscopy for measurement of water content in skin," *Skin Res. Technol.* **11**(1), 27–35 (2005).
- J. P. Culver et al., "Three-dimensional diffuse optical tomography in the parallel plane transmission geometry: evaluation of a hybrid frequency domain/continuous wave clinical system for breast imaging," *Med. Phys.* **30**, 235–247 (2003).
- M. A. Franceschini et al., "Frequency-domain techniques enhance optical mammography: initial clinical results," *Proc. Natl. Acad. Sci. U.S.A.* **94**, 6468–6473 (1997).
- T. O. McBride, B. W. Pogue, S. Jiang, U. L. Osterberg, and K. D. Paulsen, "A parallel-detection frequency-domain near-infrared tomography system for hemoglobin imaging of the breast in vivo," *Rev. Sci. Instrum.* **72**, 1817–1824 (2001).
- B. W. Pogue et al., S. P. Poplack, T. O. McBride, W. A. Wells, K. S. Osterman, U. L. Osterberg, K. D. Paulsen, "Quantitative hemoglobin tomography with diffuse near-infrared spectroscopy: pilot results in the breast," *Radiology* **218**(1), 261–266 (2001).
- D. A. Benaron et al., "Noninvasive functional imaging of human brain using light," *J. Cereb. Blood Flow Metab.* **20**(3), 469–477 (2000).
- J. P. Culver, T. Durduran, D. Furuya, C. Cheung, J. H. Greenberg, A. G. Yodh, "Diffuse optical tomography of cerebral blood flow, oxygenation, and metabolism in rat during focal ischemia," *J. Cereb. Blood Flow Metab.* **23**(8), 911–924 (2003).
- E. Gratton, V. Toronov, U. Wolf, M. Wolf, A. Webb, "Measurement of brain activity by near-infrared light," *J. Biomed. Opt.* **10**, 011008 (2005).
- D. M. Hueber et al., "Non-invasive and quantitative near-infrared haemoglobin spectrometry in the piglet brain during hypoxic stress, using a frequency-domain multidistance instrument," *Phys. Med. Biol.* **46**(1), 41–62 (2001).
- J. R. Kappa, H. D. Berkowitz, R. Seestedt, B. Chance, "Evaluation of calf muscle oxygen content. using NIRS in patients with peripheral vascular disease," *Vasc. Surg.* **1991**, 10–16 (2000).
- V. Quaresima, M. Ferrari, M. A. Franceschini, M. L. Hoimes, S. Fantini, "Spatial distribution of vastus lateralis blood flow and oxy-hemoglobin saturation measured at the end of isometric quadriceps contraction by multichannel near-infrared spectroscopy," *J. Biomed. Opt.* **9**(2), 413–420 (2004).
- L. O. Svaasand, T. Spott, J. B. Fishkin, T. Pham, B. J. Tromberg, M. W. Berns, "Reflectance measurements of layered media with diffuse photon-density waves: a potential tool for evaluating deep burns and subcutaneous lesions," *Phys. Med. Biol.* **44**(3), 801–813 (1999).
- H. W. Wang, M. E. Putt, M. J. Emanuele, D. B. Shin, E. Glatstein, A. G. Yodh, T. M. Busch, "Treatment-induced changes in tumor oxygenation predict photodynamic therapy outcome," *Cancer Res.* **64**(20), 7553–7561 (2004).
- U. Wolf, M. Wolf, J. H. Choi, L. A. Paunescu, L. P. Safonova, A. Michalos, E. Gratton, "Mapping of hemodynamics on the human calf with near infrared spectroscopy and the influence of the adipose tissue thickness," *Adv. Exp. Med. Biol.* **510**, 225–230 (2003).
- E. S. Papazoglou, M. S. Weingarten, L. Zubkov, L. Zhu, S. Tyagi, K. Pourzeaei, "Optical properties of wounds: diabetic versus healthy tissue," *IEEE Trans. Biomed. Eng.* **53**(6), 1047–1055 (2006).
- R. C. Haskell, L. O. Svaasand, T. t. Tsay, T. C. Feng, M. S. McAdams, B. J. Tromberg, "Boundary conditions for the diffusion equation in radiative transfer," *J. Opt. Soc. Am. A* **11**(10), 2727–2741 (1994).
- T. H. Pham, O. Coquoz, J. B. Fishkin, E. Anderson, B. J. Tromberg, "Broad bandwidth frequency domain instrument for quantitative tissue optical spectroscopy," *Rev. Sci. Instrum.* **71**, 2500–2513 (2000).
- I. Fridolin, K. Hansson, and L. G. Lindberg, "Optical non-invasive technique for vessel imaging: II. A simplified photon diffusion analysis," *Phys. Med. Biol.* **45**(12), 3779–3792 (2000).
- G. H. Weiss, R. Nossal, and R. F. Bonner, "Statistics of penetration depth of photons re-emitted from irradiated tissue," *J. Mod. Opt.* **36**(3), 349–359 (1989).
- H. Basu, *A Novel Method for Calibration of a Functional Near Infrared Spectroscopy (fNIRS) Instrument Used in the Assessment of Wound Healing*, Drexel University, Philadelphia, Penn. (2007).

40. N. Chbinou and J. Frenette, "Insulin-dependent diabetes impairs the inflammatory response and delays angiogenesis following Achilles tendon injury," *Am. J. Physiol. Regulatory Integrative Comp. Physiol.* **286**(5), R952–R957 (2004).
41. G. S. Sidhu, H. Mani, J. P. Gaddipati, A. K. Singh, P. Seth, K. K. Banaudha, G. K. Patnaik, R. K. Maheshwari, "Curcumin enhances wound healing in streptozotocin induced diabetic rats and genetically diabetic mice," *Wound Repair Regen* **7**(5), 362–374 (1999).
42. Institute of Laboratory Animal Resources, *Guide for the Care and use of Laboratory Animals*, National Academy Press, Washington, D.C. (1996).
43. N. Kertesz, J. Wu, T. H. Chen, H. M. Sucov, H. Wu, "The role of erythropoietin in regulating angiogenesis," *Dev. Biol.* **276**(1), 101–110 (2004).
44. G. Thurston, T. J. Murphy, P. Baluk, J. R. Lindsey, D. M. McDonald, "Angiogenesis in mice with chronic airway inflammation strain-dependent differences," *Am. J. Pathol.* **153**, 1099–1112 (1998).
45. W. G. Zijlstra, A. Buursma, and W. P. Meeuwse-van der Roest, "Absorption spectra of human fetal and adult oxyhemoglobin, deoxyhemoglobin, carboxyhemoglobin, and methemoglobin," *Clin. Chem.* **37**(9), 1633–1638 (1991).
46. G. M. Hale and M. R. Querry, "Optical constants of water in the 200-nm to 200-m wavelength region," *Appl. Opt.* **12**(3), 555–563 (1973).
47. C. Veno, T. K. Hunt, H. W. Hopf, "Using physiology to improve surgical wound outcomes," *Plast. Reconstr. Surg.* **117**(7S), 59S–71S (2006).
48. K. Jonsson, J. A. Jensen, W. H. Goodson, H. Scheuenstuhl, J. West, H. W. Hopf, T. K. Hunt, "Tissue oxygenation, anemia, and perfusion in relation to wound healing in surgical patients," *Ann. Surg.* **214**(5), 605–613 (1991).